

Vibration and structure-borne sound isolation properties of silica aerogels

Oriana Palacio^{a,*}, Wim J. Malfait^{a,*}, Silvain Michel^b, Michel Barbezat^b, Zahra Mazrouei-Sebdani^{a,*}

^a Laboratory for Building Energy Materials and Components, Swiss Federal Laboratories for Materials Science and Technology, Empa, Überlandstrasse 129, 8600 Dübendorf, Switzerland

^b Mechanical Systems Engineering, Swiss Federal Laboratories for Materials Science and Technology, Empa, Überlandstrasse 129, 8600 Dübendorf, Switzerland

ARTICLE INFO

Keywords:

Aerogel
Visco-elastic properties
Vibration damping/isolation
Structure-borne sound insulation
Vibroacoustics

ABSTRACT

Vibration reduction and structure-borne sound insulation create a healthy environment in housing by reducing the exposure of the inhabitants from sources outside or inside the building (railway and road traffic, neighbors). Current solutions include textiles, polymer foams, rubber mats and metal springs, but for many applications, highly sought after. Although thermal insulation drives the silica aerogel market, acoustic applications are increasingly gaining attention. Most acoustic studies focus on airborne sound absorption, but structure-borne sound and vibration isolation remain unexplored. In this paper, we compare the vibroacoustic properties of silica aerogel granules to those of recycled rubber and expanded cork to assess the suitability for vibration damping or vibration isolation. With a remarkably low resonance frequency (<12 Hz) and dynamic stiffness (<0.1 N/mm³), silica aerogels provide superior vibration isolation performance compared to recycled rubber (by 8 dB) over a wide range of static loads (0.02–0.12 MPa), and silica aerogel may become a viable solution for vibration isolation in construction.

1. Introduction

Aerogels are porous materials derived from a wet gel in which the pore fluid has been replaced with air while its internal structure is mostly maintained [1–5]. The large, predominantly mesoporous pore volume and the tortuosity of the nanoparticle or nanofibrous network result in a low density, a very high specific surface area, and porosity, high transparency (for SiO₂ aerogels and some biopolymer aerogels), and a very low thermal conductivity, down to 15 mW/(m·K) (Fig. 1) [5]. Aerogels can be produced from any material that can form a gel, out of which silica aerogels have been studied best, and they have by far the highest industrial production volume [6]. Despite their brittleness, silica aerogels have a wide application potential [7]. Thermal insulation has been the near-exclusive focus of the current market [8–10], e.g. in the building energy savings [11–13], oil-and-gas infrastructures [1], aerospace sector [14], and more recently, thermal barriers in lithium-ion battery packs [15]. Aside from thermal insulation, silica aerogels may also be applied for acoustic applications, which have attracted increasing attention in the last decade [16,17], but no aerogel-based acoustic insulation product has been brought onto the market so far.

Air-borne sound absorption, using an impedance tube to determine

the sound absorption coefficient (α), has been the focus of most research on silica aerogel's acoustic properties, with measurements on neat or composite silica aerogel [18–22], aerogel blanket [23–26], and silica aerogel filled fibers [27]. As sound waves propagate through the inner network of aerogels, the low-density porous structure of the material reduces sound reflections. For air-borne sound, silica aerogel's behavior is influenced by several factors, including the material form (granules, films, composites, etc.), the geometry of the network structure and/or the external boundary conditions [16,28]. On their own, silica aerogels often show a high absorption peak in a narrow range of frequencies, like sound-absorbing resonators, but inclusion of fibers leads to a smoother behavior over a wide range of frequencies more similar to sound-absorbing foams or fibrous materials. A detailed overview of the acoustic properties of silica aerogel materials is available in the review paper by Mazrouei Sebdani et al., 2020 [16].

In contrast to the numerous studies on air-borne sound absorption and insulation properties of silica aerogels [16,26,29,30], their potential for reducing vibrations or protection against structure-borne sound has not been explored yet [31]. Structure-borne sound is transmitted through foundations, walls and floors in buildings, and causes them to vibrate. In the course, sound waves can propagate through the support

* Corresponding authors.

E-mail addresses: wim.malfait@empa.ch (W.J. Malfait), zahra.mazrouei@empa.ch (Z. Mazrouei-Sebdani).

<https://doi.org/10.1016/j.conbuildmat.2023.132568>

Received 22 May 2023; Received in revised form 10 July 2023; Accepted 18 July 2023

Available online 24 July 2023

0950-0618/© 2023 The Authors. Published by Elsevier Ltd. This is an open access article under the CC BY license (<http://creativecommons.org/licenses/by/4.0/>).

structure of a building [16]. In daily life, vibration reduction and structure-borne sound insulation are important for example for a healthy environment in housing and therefore a better life quality for the habitants. Structure-borne sound in a building can be caused by sources outside of the building, such as railway or road traffic [32], as well as from sources from inside the building such as walking of neighbors (in multi-story apartment buildings) or industrial settings [33–37]. In extreme cases of for highly specialized facilities such as telescopes [38], uncontrolled vibrations can cause damage to the support structure, due to large dynamic deflections. It is thus crucial not only to minimize the excitation but also to dampen the sound wave propagation in the structures, in which elastic mounts are key elements for the isolation or damping of structure-borne sound [39,40].

The performance of a material for vibroacoustic applications can be expressed in terms of vibration damping/isolation, or structure-borne sound insulation. A determinative factor here is the natural frequency which is the frequency at which a system oscillates in the absence of an external stimulus. It depends on its stiffness and the mass involved [41,42]. While vibration-damping materials reduce the amplitude of vibrations when excited by an external stimulus oscillating with a frequency close to the natural frequency [43,44], vibration isolation materials reduce the transmissibility of vibrations over a wide range of frequencies above an excitation frequency. The critical excitation frequency is defined as $\sqrt{2}$ times the natural frequency of the system [45]. The effect of vibration-damping is most obvious near the resonance, while structure-borne sound insulation is most effective at frequencies well above the natural frequency. In practical applications of structure-borne sound insulation, lowering the natural frequency of the system to the lowest possible ensures effective insulation of a broad spectrum of noise frequencies. Considering a system of a base, a spring, and a mass, when the base and mass vibrate at the natural frequency, they move in-phase 90° apart causing the resonance, while they move out of phase above the natural frequency [46,47]. Somewhat counter-intuitively, a less strongly damped system often displays better in structure-borne sound insulation, i.e., a higher tendency for the transmissibility to more rapidly approach to zero at frequencies above $\sqrt{2}$ times the natural frequency. On the other hand, while reducing the natural frequency and therefore preventing sound waves from propagating, some damping is required to limit the amplitudes of vibrations near resonance [48,49].

Most common decoupling materials in the construction sector, e.g., polymer foams [50–52], rubber products [53–56], and textiles [57], show a combination of good vibration damping and vibration isolation

properties, both leading to structure-borne sound insulation.

Static loading is crucial to select the optimum structure-borne sound insulation or vibration isolation solution. For a floating floor with its comparatively low loads, materials such as rock wool, textiles, or compact corks are used. At intermediate to high static loads, rubber mats and highly engineered polymer foams with intermediate to high performance are used. Polyurethane foams, in particular, can be tailored to provide excellent performance for vibration isolation, albeit in a narrow static load range for a specific foam, but over a wide load range (\sim e.g., 0.01 – 2.00 N/mm²) for an entire product portfolio, i.e., a large number of different foams, each tuned for optimum performance for its narrow load range. However, these engineered polyurethane foams can be prohibitively expensive, particularly those optimized to operate at higher loads.

Despite the availability and success of current structure-borne noise and vibration damping or vibration isolation materials, there are still shortcomings in terms of performance, cost, and weight. Therefore, the investigation of alternative materials that are lighter or thinner, being able to bear high loads, and having the ability to be used under a wide range of static loads is a worthwhile endeavor. Although silica aerogels are brittle [58], they can undergo significant deformations without changing their internal structure and fully recovering from compression after load removal. This is due to their unique structure, which allows them to absorb and dissipate energy and to recover their original shape [59]. Thus, intermediate-density silica aerogels are elastic with full strain recovery after decompression [60]. This is an interesting behavior that may indicate a high potential for vibration isolation.

Here, we investigated, for the first time, the potential of silica aerogels for structure-borne sound and vibration isolation. We determined the dynamic properties, e.g. dynamic stiffness, storage modulus, loss factor, resonance frequency, and frequency response curve. We characterized two silica aerogel granule beds under a wide range of static loads and excitation frequencies, and contrasted the data to those collected on rubber and expanded cork granules using the same experimental conditions. The superior vibration isolation performance of silica aerogel granules compared to rubber and cork granules, including a very low resonance frequency over a very wide range of loads, indicate that silica aerogel may be a competitive or even superior solution for demanding vibration isolation applications in construction. Follow-up scientific research and product development strategies to convert this newly discovered potential in marketable products are proposed.

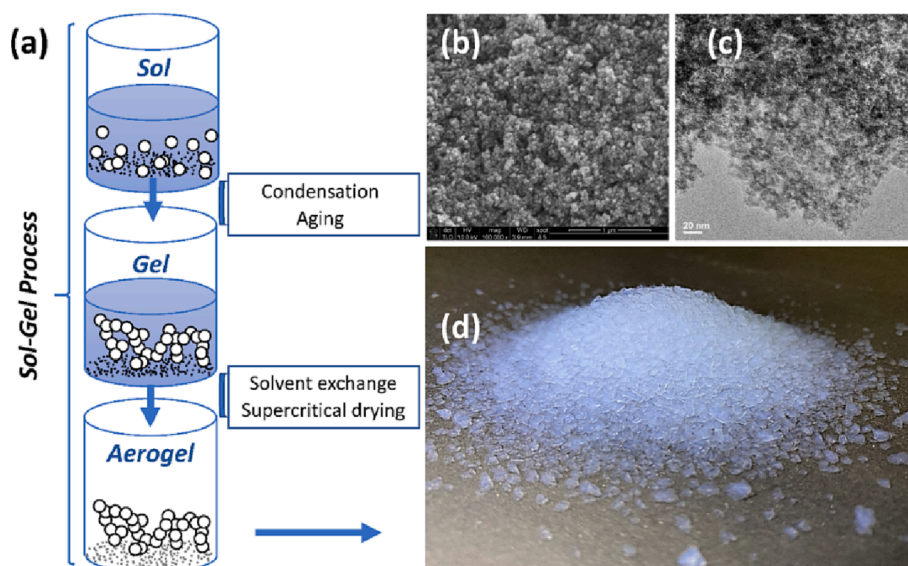


Fig. 1. Silica aerogel (a) Synthesis scheme, (b) SEM micrograph, (c) TEM micrograph, (d) Silica aerogel granules.

2. Experimental

2.1. Study design and approach

This is an experimental study on the vibro-acoustic properties of silica aerogel granules. In order to compare and contrast the materials' performance, recycled rubber and expanded cork granules of similar grain sizes were also evaluated using identical measurement conditions. All materials were sourced commercially from important players in the market, hence the materials are suitable representatives of their materials class. The main characterization techniques are forced vibration measurements with the following variables: static load and vibration amplitude and frequency, and the data are interpreted within the single degree of freedom framework. Because the forced vibration measurements may induce changes in the sample, the grain size and microstructure were evaluated carefully before and after the measurements.

2.2. Materials

Silica aerogel (SA) granules from Cabot corporation (USA, P300 and P200), recycled rubber (RR) coarse powder (0.5–0.8 mm) and granulate (1–3 mm) from Genan (UK), and expanded cork granules from HAGA AG Naturbaustoffe (Switzerland) were selected for characterization and evaluation of structure-borne noise and vibration damping properties. The names of the materials were abbreviated according to Table 1. Later, the code “abbreviation”-“sample thickness” will be used to present the results in all the figures, e.g., data marked SA P200 – 70 mm is derived from a bed of a 70 mm thick bed of P200 silica aerogel granules. Rubber and cork materials are traditional materials for vibration and structure-borne noise insulation; the specific grades were selected to be of a particle size similar to those of the studied aerogels. They were evaluated as benchmark materials for the aerogels studied. A graphical comparison of the size of the granules is shown in Fig. 2.

2.3. Characterization

2.3.1. Basic characterization

The tap density (mass by volume) of the granules was measured by weighting an amount of material (Mettler Toledo AG204 Delta Range® Analytical Balance) in a measuring cylinder and determining the volume after 1000 taps applied with a tapping machine (Jolting volumeter STAV II, J. Engelsmann AG, F). The uncertainty of the tap density is estimated to be $\pm 5\%$. The envelope or bulk density was measured using a powder pycnometry device in the GeoPyc 1360 machine (Micrometrics Co., Germany). Particles around 2 mm (and around 1 mm for the finest materials) were selected, and sufficient material was used to ensure that the sample volume was around 1/3 of the volume of the calibration sand. A low consolidation force of 4 N was used for each measurement to avoid excessive compression during the measurement. The uncertainty on the envelope density is estimated to be $\pm 4\%$.

The microstructure was probed by nitrogen sorption analysis (3Flex, Micrometrics). The Brunauer–Emmett–Teller (BET) and Barrett–Joyner–Halenda (BJH) methods were used to estimate the surface

area and pore size distribution of the aerogels, with estimated uncertainties of $\pm 10\%$ on the surface area. Approximately 100 mg of the sample was degassed at a vacuum pressure of 0.016 mmHg for 10 h at 120 °C (temperature ramp rate of 10 °C/min). Weight of the dry sample was measured afterward. The nitrogen sorption isotherms were acquired at P/P_0 values between 0.001 and 0.998 in 30 steps. Pore size determinations of aerogels by nitrogen sorption analysis suffer from several artifacts: Only pores below 50–100 nm are sampled and complications arise from sample deformations during nitrogen sorption (capillary forces) [61]. Pore volume (V_{pore}) and average pore diameter (D_{pore}) were therefore estimated from the envelope and skeletal density ($\rho_{envelope}$ and $\rho_{skeletal}$, respectively). The surface area was determined by assuming cylindrical pores and a skeletal density of 2.0 g/cm³.

The particle size distribution was determined with a Rotary Sieve Shaker, Analysette 18 - model 1991 (Fritsch GmbH Company, Idar-Oberstein, Germany). It was used to separate the size fractions by a stack of five sieves for each material, selected from standard sieves according to ISO 3310-1 of pore size 4 mm, 2.8 mm, 2 mm, 1.4 mm, 1 mm, 0.5 mm, 0.25 mm, 0.125 mm, and 0.09 mm. The sieves were preselected to cover a size range close to that established by the manufacturers. Each material was shaken in the sieve stack for 5 min at a shaker speed of 6 out of 10; for the aerogel, half this speed was used to avoid damaging the aerogel grains. Finally, the fractions of each material were weighted in a Mettler Toledo PR5002 Delta Range® Analytical Balance.

The static compression/decompression behavior of the granulate beds was evaluated in a Zwick machine BZ100/TL35 according to the standard EN 826. Each sample was loaded to 40% strain after a 20 N preload to ensure contact with the plates. The granules of the materials were put inside a mold of 20 × 20 cm², and a deformation rate of 5 mm/min was used for the measurements. The nominal inter-granular porosity, i.e. the pore volume in between the aerogel grains (assuming that the grains themselves do not compress) was calculated from the initial packed bed density ($\rho_{0,bed}$), the strain (ϵ) and the aerogel envelope density ($\rho_{envelope}$, 0.109 and 0.134 g/cm³ for P200 and P300, respectively) as $1 - [\rho_{0,bed}/(1 - \epsilon)] / \rho_{envelope}$.

The stress relaxation and creep response were evaluated on the Instron® 1273 machine with an assembly similar to that of the compression tests. In the stress relaxation test, a constant deformation equivalent to a strain of 40% was imposed at a speed such that the desired deformation of the specimen is reached in 3 s, and the load response was measured for 1 h. In the creep response test, a constant force of 4000 N was imposed, and the deformation was measured during 1 h.

2.3.2. Vibroacoustic measurements

The vibration isolation, as well as vibration damping performance, was evaluated on the Instron® 1273 machine (Instron® Company, Massachusetts, USA) according to the standard DIN 53513. The set-up used for the vibroacoustic test is shown in Fig. 3a. A specimen is mounted between two steel plates (20x20 cm²) and first subjected to a static load, i.e. a constant pressure. The specimen is then exposed to deformation oscillations with a predetermined amplitude and frequency in the normal direction as shown in Fig. 2c. The following conditions were tested: oscillation frequency of 5 and 10 Hz (each with an amplitude of 0.125 mm, 0.25 mm, and 0.3 mm) and 30 Hz with an amplitude of 0.04 mm, 0.08 mm, and 0.25 mm). This resulted in nine frequency-amplitude combinations. The following mean loads are evaluated: 80, 100, 200, 300, 400, 500, 600, 800, 1000, 1200, and 1400 N for each frequency-amplitude combination, corresponding to uniaxial pressure between 2 and 35 kPa. Having seen the good performance of the silica aerogels at higher loads in the first set of measurements, the load range was extended to 5000 N or 125 kPa in a second set of measurements. In this study, mainly the results for the frequency-amplitude combination of 10 Hz – 0.25 mm will be presented, based on the standard conditions reported in the protocol DIN 53513. To compare the effect of oscillation frequency and amplitude, some results were graphed for the other

Table 1

Sample code and material specifications of the investigated granules according to the manufacturers.

Sample code	Material description
SA P200	Silica aerogel P200, size 0.1–1.2 mm, S_{BET} : 600–800 m ² /g, d_{pore} 20 nm, ρ_{tap} 75–95 kg/m ³ , $\Phi > 90\%$
SA P300	Silica aerogel P300, size 1.2–4.0 mm, S_{BET} : 600–800 m ² /g, d_{pore} 20 nm, ρ_{tap} 65–85 kg/m ³ , $\Phi > 90\%$
RR 0.5–0.8 mm	Recycled rubber coarse powder, size 0.5–0.8 mm
RR 1–3 mm	Recycled rubber granules, size 1–3 mm
Cork	Expanded cork granules, size 2–4 mm

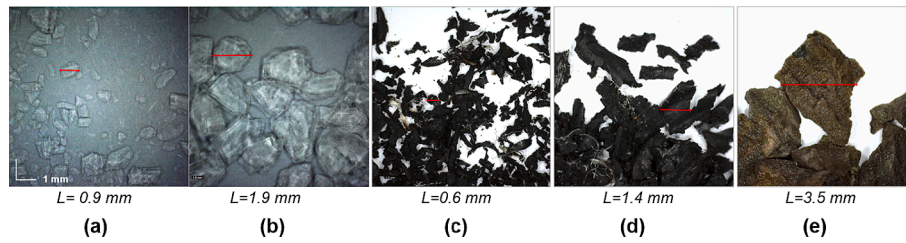


Fig. 2. Tested materials: (a) SA P200, (b) SA P300, (c) RR 0.5–0.8 mm, (d) RR 1–3 mm, and (e) expanded cork. All images have the same magnification (35x, scale bare shown on the left).

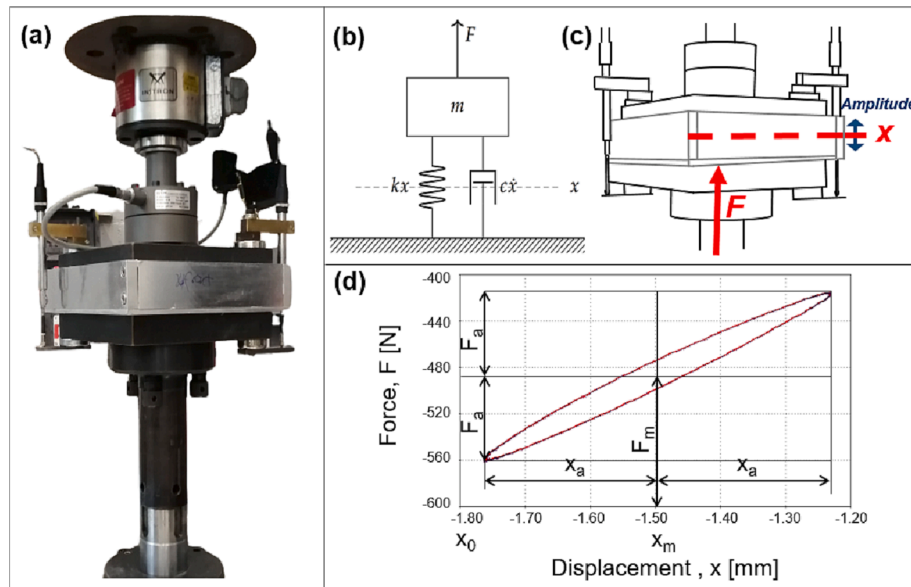


Fig. 3. (a) Vibroacoustic test set-up; (b) Mass-spring-damper system; (c) Close-up of the mass-spring-damper system on the test set-up (d) Force-displacement diagram for a test with 500 N static load, a vibration frequency of 10 Hz and a displacement amplitude of 0.25 mm.

conditions as well. The uncertainties can be estimated from the standard deviation of the results from repeated experiments (using virgin material under the same conditions): The uncertainty of the resonance frequency was determined to be within ± 0.5 Hz and the uncertainty for the dynamic stiffness and storage modulus were $\sim \pm 5\%$. The uncertainty of the loss factor was substantial at low static loads, e.g. up to $\pm 20\%$, for loads below 0.01 N/mm^2 , but only $\sim \pm 10\%$ for loads above 0.01 N/mm^2 .

In addition to the measurements of the dynamic response with off-resonance forced excitations, frequency sweeps from 1 to 60 Hz were carried out at selected static loads to determine the transmissibility response with respect to the frequency. Note that we did not measure the transmissibility directly, but calculated it for each imposed oscillation from the resonance frequency and the damping ratio (both measured at the same frequency) using Eq. (10) (see below). Here we assumed the test set-up and the specimen to behave as a single-degree-of-freedom (SDOF) mass-spring-damper system.

2.3.3. Principles of the oscillation system operation & derivation of the relevant parameters

Characterization of oscillatory systems in practical applications is made by fitting a simplified mechanical model. For many vibration problems, it is sufficient to use a one-dimensional model of a mass-spring-damper system. This model does not account for out-of-plane movements. In such models, the oscillating body can be represented by a number of discrete individual masses linked by pairs of springs and dampers connected in parallel. The number of independent movement options is referred to as degrees of freedom (DOF). DOF is also equal to the number of possible natural frequencies of the system. For measuring

vibration isolation, in general, the lowest natural frequency is the most relevant one. Because it is approximately the same for all models fitted to the system analyzed, a one-dimensional mass-spring-damper model is often sufficient. This type of model has therefore been selected here. In a single-degree-of-freedom (SDOF) mass-spring-damper system according to Fig. 3b,c, the specimen is represented by a spring with stiffness k in parallel with a damper with a damping constant c [62]. The mass m is the mass of the upper plate. The values of k and c are functions of the applied mean load F_m . $F(t)$ is the applied force (mean load plus cyclic force), and $x(t)$ is sinusoidal cyclic deformation. While in the test the mean load and the sinusoidal cyclic deformation are controlled, the static deformation and the dynamic force response are measured. The resulting force–displacement behavior is illustrated in Fig. 3d, where F_m and F_a are the mean force and force amplitude in [N], respectively, x_0 is the thickness of the sample before testing [mm], x_a is the amplitude of the deformation [mm], and x_m is the mean deformation [mm].

The determination of the vibroacoustic properties was attained by exposing the samples to forced vibrations at non-resonant frequencies. With this method, it is possible to measure the dynamic (viscoelastic) properties. With these properties, it is then possible to predict the behavior of materials when a sinusoidal deformation is applied. For a combination of frequency and stress amplitude, the strain response and the storage modulus of the elastic-spring damper system can be calculated.

The motion of a one-degree-of-freedom (1-DOF) vibrating system follows equation (1).

$$m\ddot{x}(t) + c\dot{x}(t) + kx(t) = F(t) \quad (1)$$

where, m is the mass (kg), c the coefficient of viscous damping (kg/s), k the spring coefficient (N/m), and $F(t)$ is an external force. Eq. (1) can be rewritten as Eq. (2).

$$\ddot{x}(t) + 2\xi\omega_0\dot{x}(t) + \omega_0^2x(t) = F(t) \quad (2)$$

in which, parameters of the circular natural frequency of ω_0 , the natural frequency of f_0 and damping ratio of ξ are defined as Eqs. (3) and (4):

$$\omega_0 = \frac{1}{2\pi}f_0 = \sqrt{k/m} \quad (3)$$

$$\xi = \frac{c}{2\sqrt{mk}} \quad (4)$$

In an undamped system $\xi = 0$, in an underdamped system $0 < \xi < 1$, in a critically-damped system $\xi = 1$, and in an overdamped system $\xi > 1$.

A 1-DOF system mounted on a fixed foundation can be subject to harmonic excitations. The equation of motion of the system follows Eq. (5).

$$m\ddot{x}(t) + c\dot{x}(t) + kx(t) = F_0\sin\omega t \quad (5)$$

The natural or resonance frequency $f_0(\sigma_m, f)$ in [Hz] can be calculated based on the dynamic stiffness $c(\sigma_m, f)$ [N/mm³] according to the formulas (6) and (7).

$$c(\sigma_m, f) = \frac{\sigma_a}{x_a} \quad (6)$$

where σ_a is the stress amplitude in [N/mm²], and x_a is displacement amplitude in [mm] as shown in Fig. 2 (d).

$$f_0(\sigma_m, f) = \frac{1}{2\pi} \sqrt{c(\sigma_m, f) \times g/\sigma_m} \quad (7)$$

The earth's gravity constant is represented with g [mm/s²], σ_m is the mean stress [N/mm²].

In our tests, the mean force (F_m) and the amplitude were kept constant for each measurement, while the associated force response (F_a) was measured.

The mechanical loss factor d is given by the Eq. (8) and the complex (dynamic) modulus $|E^*|$ by Eq. (9):

$$d = \tan(\delta) \quad (8)$$

where δ specifies the lag between the strain and stress signal or the phase difference over time.

$$|E^*| = \frac{\sigma_a}{\varepsilon_a} = \frac{F_a}{L_a} \times \frac{L_0}{A_0} \quad (9)$$

where σ_a is stress amplitude, and ε_a is the associated strain amplitude. Given that $\sigma_a = F_a/A_0$ and $\varepsilon_a = L_a/L_0$, where A_0 is the cross-sectional area of the tested sample. It is possible to calculate the complex modulus from the parameters measured on the specimen during the test [63].

As for vibration isolation, the key property of the system is transmissibility (transmission ratio $|F_{TR}/F|$), which can be simplified according to Eq. (10). It depends on the natural frequency and damping ratio of a 1-DOF system. Vibration isolation occurs when $TR < 1$, which will be at $\sqrt{2}$ of natural frequency and above (Fig. S1). According to this relation, and borne out by experimental data, lower damping ratios lead to lower transmission function at higher frequencies and are thus preferable for vibration isolation [45]. However, some damping is also needed to limit resonance at lower frequencies. It is common for elastomers to exhibit both good vibration isolation and vibration damping and subsequently, good noise insulation behavior. The right compromise between acceptable damping and high isolation can be found by selecting (or developing) materials with specific parameters according

to use conditions, specific loads, and vibration probability.

$$\text{Transmissionfunction} = \left| \frac{F_{TR}}{F} \right| = \sqrt{\frac{1 + (2\xi\frac{f}{f_0})^2}{(1 - \frac{f^2}{f_0^2})^2 + (2\xi\frac{f}{f_0})^2}} \quad (10)$$

The damping behavior can also be described in terms of the mechanical loss factor η , which is a measure of the difference between the resonance frequency and the natural frequency of a mass-spring system:

$$f_R = f_0 \sqrt{1 - \eta^2} \quad (11)$$

where f_R is the resonance frequency and f_0 natural frequency. A material with a high loss factor has a lower resonance frequency than the natural frequency, while a material with a low loss factor performs vice versa [64]: As the loss factor increases, the resonance frequency decreases [65]. The mechanical loss factor η is double the damping ratio ξ . Here, due to considering a mass-spring-damper system, Eq. (7) gives the resonance frequency, which is shown in the graphs.

3. Results and discussion

3.1. Structural and physical properties

The cumulative particle size distribution of all materials measured before the vibroacoustic test is presented in Fig. 4a, and the cumulative particle size distribution of the SA before and after the vibroacoustic test is presented in Fig. 4b. Consistent with the datasheets from the manufacturer, most particle sizes in aerogel P200 are < 1 mm, but between 1 and 3 mm in aerogel P300. The static force and deformation oscillations to which the samples are subjected during the measurement of vibroacoustic properties strongly reduce the particle sizes for the course P300 silica aerogel, with a much more modest effect for the finer P200 silica aerogel. The effect of the vibroacoustic testing on reducing the particle size is also more pronounced when a thinner sample had been measured (35 versus 70 mm). The reduction in particle size during the vibroacoustic testing means that the sample state changes progressively as the load is increased and the measurement progresses. However, the effect of this change in the particle size of the sample on the vibroacoustic properties is not expected to be very large, given that particle size has no significant effect on the vibroacoustic properties in any case (see Section 3.2).

The physical characterization of materials is reported in Table 2. The pore volume (V_p) was determined in two different ways. Table 2 reports the total pore volume V_p calculated from the difference of the inverses of the envelope density (ρ_{envelope}) and the skeletal density (ρ_{skeletal}): $V_p = 1/\rho_{\text{envelope}} - 1/\rho_{\text{skeletal}}$. This pore volume includes all the pores in the system (macro-, meso- and micropores). From this pore volume and the specific surface area (S_{BET}), the average pore diameter D_p was calculated assuming cylindrical pores: $D_p = 4V_p/S_{\text{BET}}$.

On the other hand, Table 3 reports the experimental $BJHV_p$ values obtained by nitrogen sorption analysis and BJH analysis. Note that nitrogen sorption analysis is not sensitive to macropores, hence the BJH pore volumes only include the meso- and microporosity, where the latter is not substantial for silica aerogels. The specific surface area (S_{BET}) was characterized before and after the vibroacoustic testing to evaluate the possible effects of the compression in the oscillation system on the microstructure of the material (Table 3). Specifically, the surface area and pore size were measured on separate size fractions, including the fines (> 0.25 mm for SA P200 and > 1 mm for SA P300) and coarse fractions (> 1 mm for SA P200 and > 2 mm for SA P300), to assess how they were particularly affected and if there were changes in microstructure of the silica aerogel.

Based on the results presented in Table 3, the vibroacoustic testing does not have a significant effect on the microstructure of the aerogels (neither on the surface area nor on the volume of the pores. This is in contrast to the observed effects on the particle size distribution (Fig. 4).

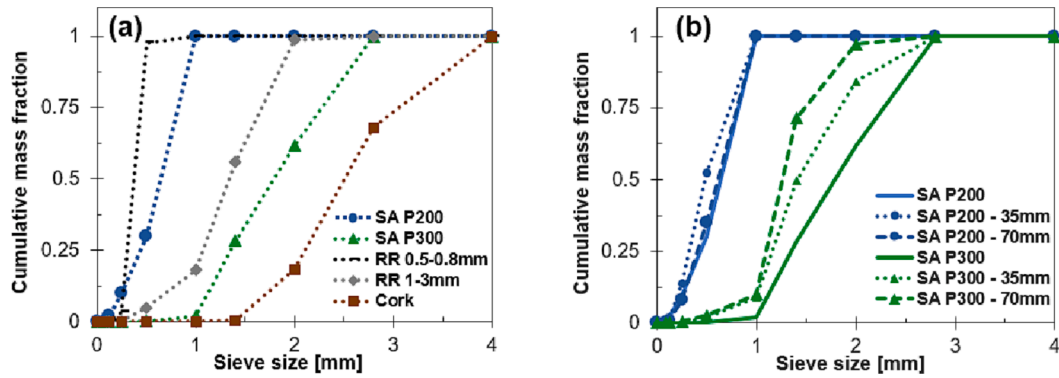


Fig. 4. Particle size distribution diagram of (a) all materials before the vibroacoustic test, and (b) SA P200 and SA P300 before and after the vibroacoustic test.

Table 2

Densities and porosity.

Material	Particle size [mm]*	Tap density [g/cm ³]	Envelope density [g/cm ³]	Skeletal density [g/cm ³]	Pore volume (Vp) [cm ³ /g]	Pore diameter (Dp) [nm]
SA P200	0.1–1.2	0.082	0.109	2.2	8.7	48.6
SA P300	1.2–4.0	0.068	0.134	2.2	7.0	39.6
RR 0.5–0.8 mm	0.5–0.8	0.458	1.084	n.a.	n.a.	n.a.
RR 1–3 mm	1.0–3.0	0.505	1.084	n.a.	n.a.	n.a.
Cork	2.0–4.0	0.064	0.141	n.a.	n.a.	n.a.

*Nominal particle size reported by the supplier. n.a.: not analyzed. The BET surface-area test was possible only for aerogels, which are mesoporous.

Table 3

BET surface area and BJH pore volume for silica aerogel before and after vibroacoustic testing.

	Silica Aerogel P200					Silica Aerogel P300				
	Before test	Tested – 35 mm		Tested – 70 mm		Before test	Tested – 35 mm		Tested – 70 mm	
		Fine	Coarse	Fine	Coarse		Fine	Coarse	Fine	Coarse
BET surface [m ² /g]	717	717	779	734	721	706	695	667	686	710
BJH Vp [cm ³ /g]	3.2	3.2	3.5	3.2	3.2	3.2	3.2	3.1	3.1	3.3

The same invariance can also be observed in the adsorption isotherms themselves, which display no differences in the shape, hysteresis, and intensity of the isotherms (Fig. 5).

3.2. Vibroacoustic behavior

3.2.1. Resonance frequency

The resonance frequency results for the different materials are presented in Fig. 6. For all investigated materials, there is a strong initial decrease in resonance frequency with increasing specific load up to ~ 0.01 N/mm², followed by a much more gradual decrease at higher loads. The resonance frequency of both tested aerogels (P200 and P300)

is significantly lower, i.e., the performance is significantly better than that for the rubber and cork, which are commonly used for vibration isolation. Both aerogel particle sizes surpass the performance of the best rubber material (RR 0.5–0.8 mm). A minimum natural frequency value of around 14 Hz is obtained with SA with 35 mm thickness for intermediate to high loads, which is 11 Hz with 70 mm thickness, about 4 Hz lower than for the recycled rubber.

For a given thickness and static load, the P200 and P300 aerogels show the same resonance frequency over the entire range up to 0.35 N/mm². This means that the particle size distribution has a negligible effect on the dynamic properties of the silica aerogel. For the recycled rubber granules, there is a small, but systematic effect, with lower resonance

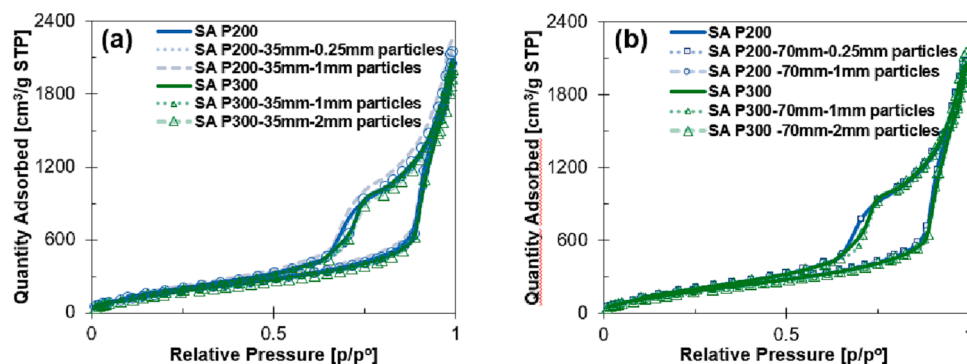


Fig. 5. Nitrogen sorption isotherms for SA P200 and SA P300 before and after the vibroacoustic test for (a) the 35 mm sample and (b) the 70 mm sample in different fractions of the material. Legend: “material abbreviation”-“sample thickness”-“material fraction”.

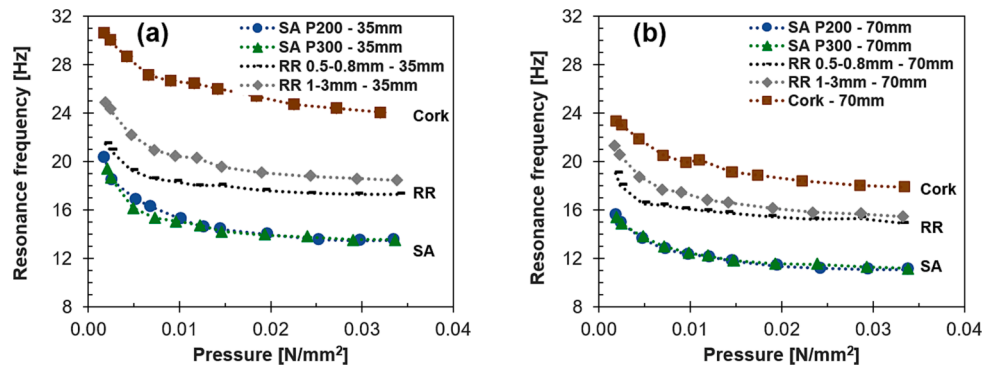


Fig. 6. Resonance frequency measurement for aerogel, rubber, and cork granule beds of (a) 35 mm, and (b) 70 mm thickness.

frequencies for smaller particle sizes. Both aerogel grades have near identical microstructures but significantly different particle sizes (Table 3), hence the independence of particle size provides a first indication that the microstructure is the reason for the better performance of aerogels compared to rubber and cork materials.

Since the resonance frequency of a mass-spring-damper system is a function of the imposed vibration, the influence of the selected imposed frequency on the resonance frequency was investigated. The main goal was to clarify the question if the low resonance frequency is reproducible under different imposed loading: An amplitude sweep of 0.05–0.35 mm (at 10 Hz) (Fig. 7a) and a frequency sweep of 5–30 Hz (at an amplitude of 0.1, 0.25 and 0.3 mm) (Fig. 7b) were selected. This is in a typical range of vibrations in civil engineering construction. The tests were carried out in an oscillatory system with the same applied pressure as in a support of a building. A static load of 0.012 N/mm² (500 N for our sample area of 400 cm²) was selected as from this load onwards, the samples showed a low and roughly constant resonance frequency. An increase in the amplitude of around 0.3 mm leads to a decrease in resonance frequency of around 12% (Fig. 7a). Conversely, the resonance frequency increases with a higher imposed frequency from 5 to 30 Hz by around 6% for an amplitude of 0.1 mm and 16% for an amplitude of 0.3 mm. In summary, a higher amplitude leads to somewhat a lower resonance frequency, whereas a higher imposed frequency increases the resonance frequency. Additional data on the effect of the deformation amplitude on the resonance frequency over a wide load range are shown in Fig. S2. In the following, we report the data for a frequency of 10 Hz and amplitude of 0.25 mm (marked in red in Fig. 7), for which the oscillation system has a good response to these conditions for the granules studied.

3.2.2. Dynamic stiffness and dynamic modulus

The dynamic stiffness and dynamic modulus (ratio of stress to strain under vibratory conditions) can be derived from the same dataset from which the resonance frequencies were calculated. We report both values

because, in different fields of application, the performance data are either reported as dynamic modulus (e.g., under-screed structure-borne noise insulation) or resonance frequency (e.g., vibration isolation). The relationship between the dynamic stiffness and the resonance frequency is given by Eq. (7). Materials with higher dynamic stiffness (and higher dynamic modulus) have normally higher resonance frequencies [66]. Thus, consistent with the resonance frequency data above (Fig. 6), the silica aerogel granule beds display a lower dynamic modulus and dynamic stiffness than the recycled rubber and expanded cork (Fig. 8).

3.2.3. Loss factor

When damping materials are subjected to dynamic loading, some of the mechanical work applied is transformed into heat (dissipation) [67]. The loss factors can be derived from the same dataset as the resonance frequencies and dynamic moduli, but typically with higher uncertainties than for the other parameters. The loss factors of the silica aerogel granule beds rapidly decrease with increasing static loads and level off at around 0.15 for static loads above 0.01 N/mm² (Fig. 9). In contrast, the loss factors of the recycled rubber and the expanded cork granule beds are less dependent on static loading. However, they are overall higher by a factor of around 2. Whereas the resonance frequency and dynamic modulus were independent of the grain size of the silica aerogel, the loss factor seems to be consistently lower for the aerogel with larger particles (P300). The low loss factor, and hence the low damping ratio of the silica aerogels means that silica aerogels are not strong vibration damping material. As a consequence, the amplitude at resonance will be higher than for rubber or cork materials. However, at higher frequencies (above $\sqrt{2}$ times resonance frequency), the lower loss factor will lead to lower transmissibility and better vibration isolation performance compared to recycled rubber and expanded cork, which are common materials for vibration isolation.

3.2.4. Forced vibrations at higher static loads

Because the resonance frequency of the silica aerogel granule beds

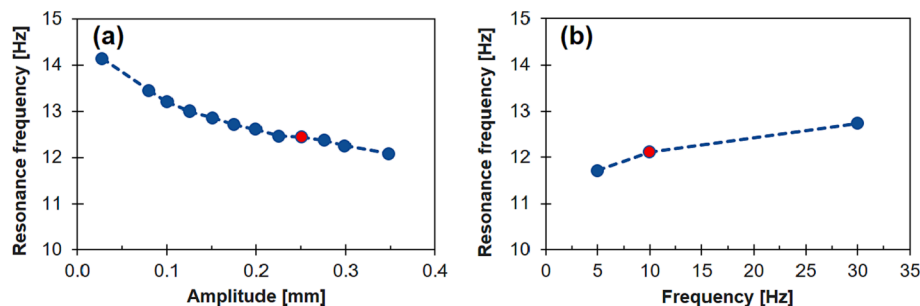


Fig. 7. Resonance frequency as a function of vibration amplitude and frequency, determined by off-resonance forced vibration measurements of SA P200, 70 mm thickness, at a static pressure of 0.012 N/mm². (a) Amplitude sweeps at a vibration frequency of 10 Hz, and (b) Frequency sweeps at a vibration amplitude of 0.25 mm.

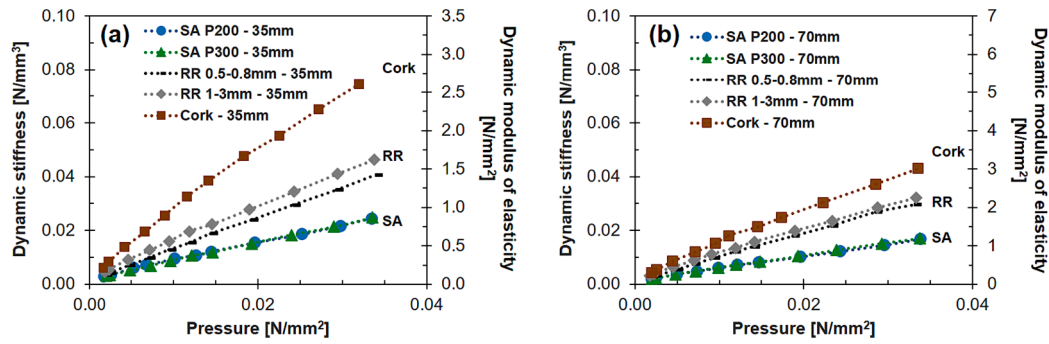


Fig. 8. Dynamic stiffness and dynamic (complex) modulus for granule beds of (a) 35 mm, and (b) 70 mm thick aerogels, determined in off-resonance forced vibration tests.

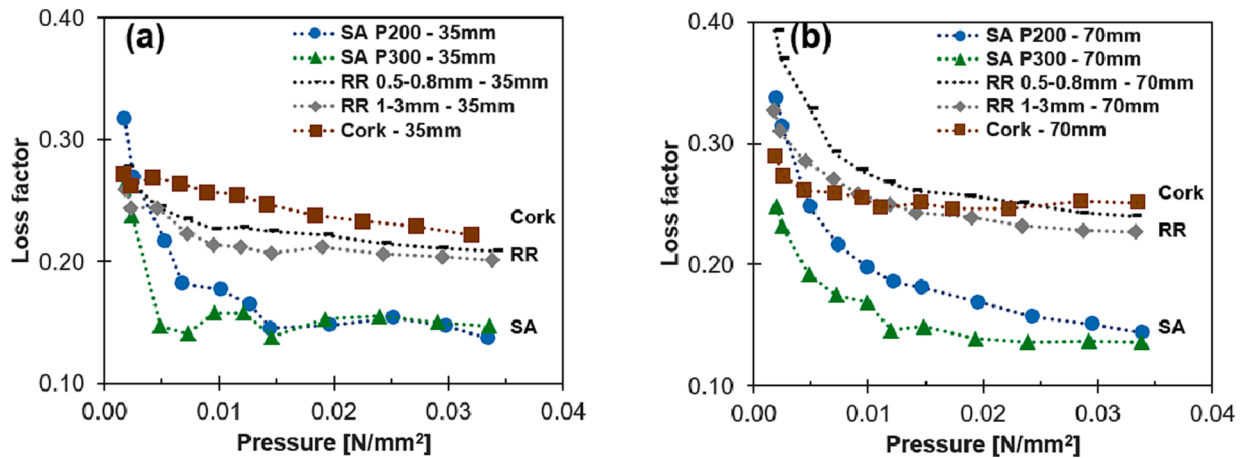


Fig. 9. Loss factor for granules of (a) 35 mm, and (b) 70 mm thick aerogels, determined in off-resonance forced vibration tests.

decreased over the investigated static loading up to 0.035 N/m^2 (without the frequently seen increase at higher loads, for example in highly engineered polyurethane foams) we decided to extend the pressure range up to 0.125 kPa (0.125 N/m^2). The data illustrate that the resonance frequencies remain very low even over this extended load range (Fig. 10a, b). This behavior is surprising and is in strong contrast to the highly engineered polyurethane foams. Those materials show their high performance (i.e., low resonance frequency) only in a narrow band of loading. In the aerogel materials however the dynamic stiffness and modulus continue to increase with increasing load, without an obvious change in slope over the investigated pressure range (Fig. 10c, d). The loss factor data of the extended pressure range also show no major variations at elevated pressures (Fig. 10e, f). The aerogel data shown here indicate that silica aerogels have remarkable constant vibroacoustic properties and over a wide range of loading a very low resonance frequency.

3.2.5. Frequency response functions of silica aerogels

The off-resonance forced vibration data (Figs. 6–10) indicate that silica aerogels have a low resonance frequency and a low loss factor. This behavior is nearly independent of the static loading, which has been shown over a very large static load range. It indicates a high potential for vibration isolation applications. Encouraged by these results, we investigated the frequency response functions for selected static loads for the P300 silica aerogel and the higher performing, finer recycled rubber (RR 0.5–0.8 mm) (Fig. 11, S3). Consistent with the lower loss factor determined by the off-resonance vibration tests (Fig. 9), the silica aerogel displays a stronger resonance than the recycled rubber: The peak at resonance is much narrower and the amplification is by a factor of up to 10 larger in the aerogels compared to the rubber, which shows only an

amplification factor of about 5. The resonance frequency determined from the maximum in amplification (Fig. 11, S3) is consistent with the off-resonance forced vibration test data (Fig. 6): For a given sample thickness, the silica aerogels have a resonance frequency that is about 4 Hz lower for the silica aerogel than for the recycled rubber. Consistent with the 1-DOF theory, the combination of a low resonance frequency and a low damping ratio results in an excellent vibration isolation performance at frequencies beyond $\sqrt{2}$ times the resonance frequency. The silica aerogels are therefore effective vibration isolators for frequencies above 16 and 20 Hz, for a thickness of 70 and 35 mm, respectively. Although the resonance frequency of 35 mm thick silica aerogels is very close to that of a 70 mm thick specimen made of recycled rubber granules by coincidence, the vibration isolation performance of the 35 mm thick silica aerogel is better by about 4 dB due to its lower damping ratio. For the same thickness, the silica aerogel provides better vibration isolation than the recycled rubber by about 8 dB, which is close to an order of magnitude. The frequency response functions acquired at different static loads (Fig. S3) confirm the excellent vibration isolation performance of the silica aerogels over a wide range of static loading.

3.3. Static compression/decompression and stress/strain relaxation

After completing the vibroacoustic characterization, we considered the state of the granule bed during a strong static compression-decompression cycle. All investigated materials (silica aerogels, recycled rubber, and expanded cork) display similar stress-strain curves during this cycle, with a substantial hysteresis and an incomplete strain recovery after full load release. This effect is due to the increased packing efficiency of the granules during compression. The strain under static, uniaxial compression of the silica aerogel beds is very similar for

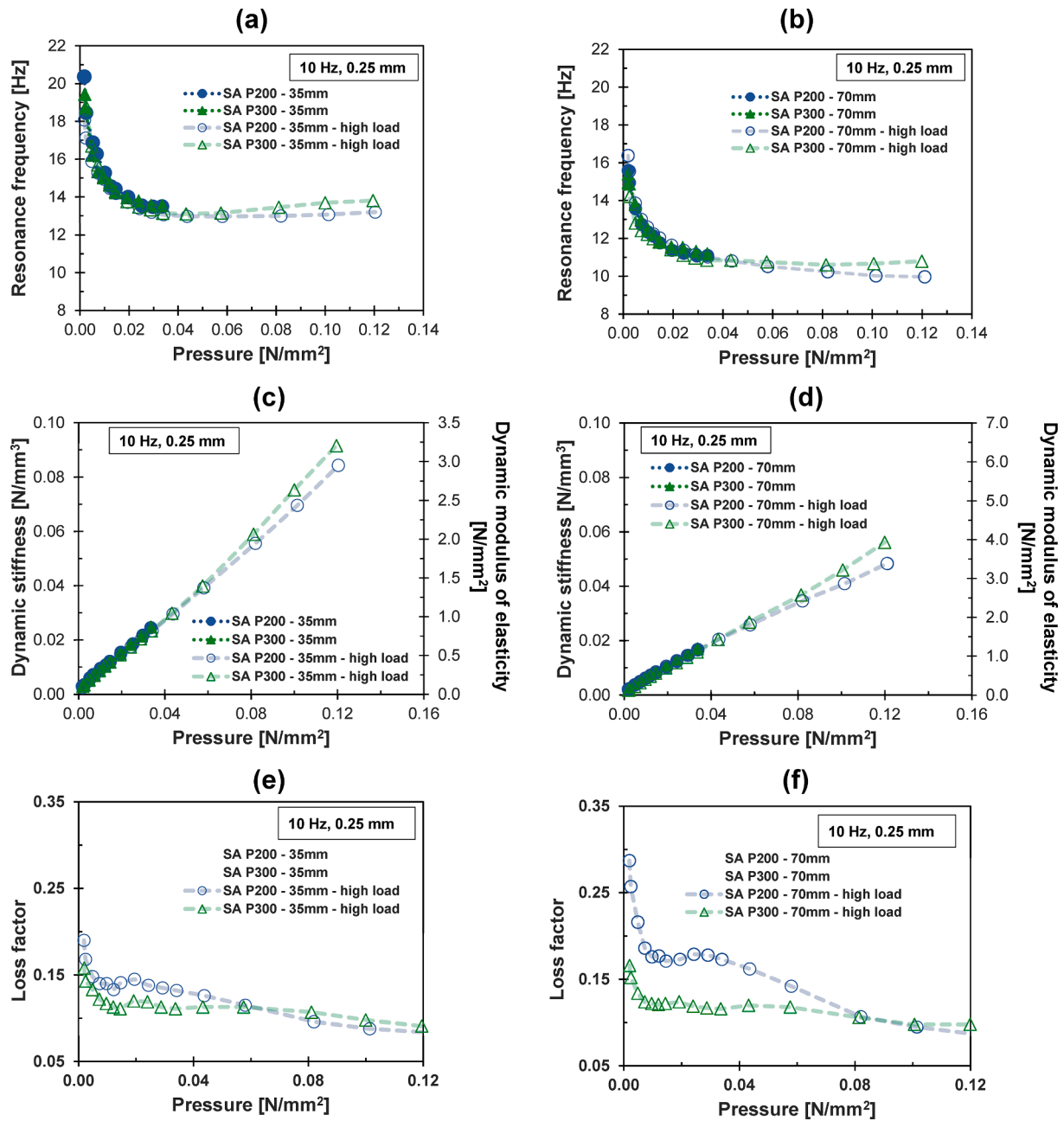


Fig. 10. Off-resonance forced vibration tests at static loads up to 0.12 N/mm². Resonance frequency for samples with thicknesses of (a) 35 mm, and (b) 70 mm. Dynamic stiffness and dynamic modulus for aerogel granules for samples thicknesses of (c) 35 mm, and (d) 70 mm. Loss factor for aerogel granules thicknesses of (e) 35 mm, and (f) 70 mm.

the P200 and P300, but quite substantially different at 23, 33 and 40% compression with a load of 0.025, 0.050, and 0.075 N/mm², respectively.

Static compression-decompression loading cycles with beds of silica aerogel granules have been investigated in quite some detail [68]. Two densification mechanisms act during the compression of a packed bed of silica aerogel granules, as observed by in situ X-ray tomography [68]. During the first stages of compression, the silica aerogel granules reduce in particle size (Fig. 4) and rearrange accompanied by an increase in packing efficiency. This can be quantified by the amount of reduction of the free, inter-granular pore volume: The pores between the aerogel grains get smaller and are filled with fragments of broken larger granules. In a second step, at higher levels of compaction, this mechanism alone can no longer keep up with the increasing strain, and the aerogel granules themselves densify even more through a reduction of the intra-

granular pore volume. The strain range at which this compression mechanism becomes dominant depends on compressive modulus, the brittleness of the silica aerogel, and the density of the packed bed before compression. However, at the very latest stage, the densification of the silica aerogel itself must occur once the nominal inter-granular porosity becomes negative (Fig. 12b, S4), i.e., once the packed bed density becomes equal to the uncompressed envelope density of the silica aerogel granules. In addition to these changes in particle size and particle arrangement, in situ X-ray tomography during compression of silica aerogel beds [68], indicates that at intermediate and high strain values, the contact area between the granules increases.

Note that most of the changes in the vibroacoustic properties (e.g., resonance frequency, loss factor) occur in the strain regime where the dominant compression mechanism is a reduction in the inter-granular porosity, with almost no further changes at higher strain values where

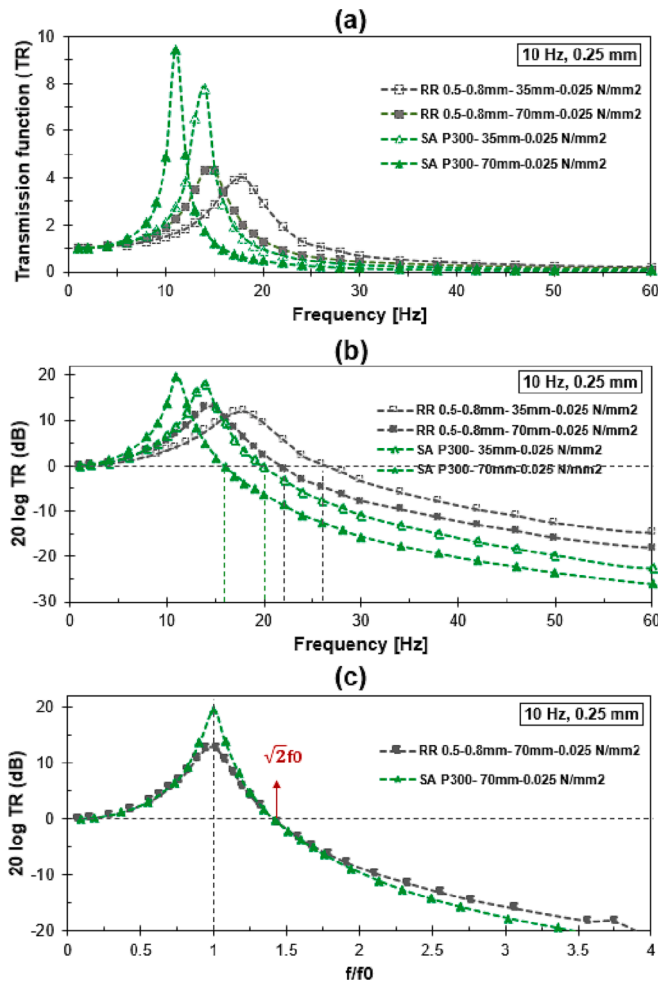


Fig. 11. Transmissibility as a function of imposed frequency at a static load of 0.025 N/mm² and deformation amplitude of 0.25 mm (determined using Eq. (10)); (a) linear and (b and c) logarithmic plot. The frequency response functions for additional static loads are given in Fig. S3.

the densification of the aerogel grains itself is dominant. Thus, the low resonance frequency is a feature of the silica aerogel itself, rather than a feature associated with the form of the granules. This is consistent with the demonstrated insensitivity of the vibroacoustic properties on the particle size.

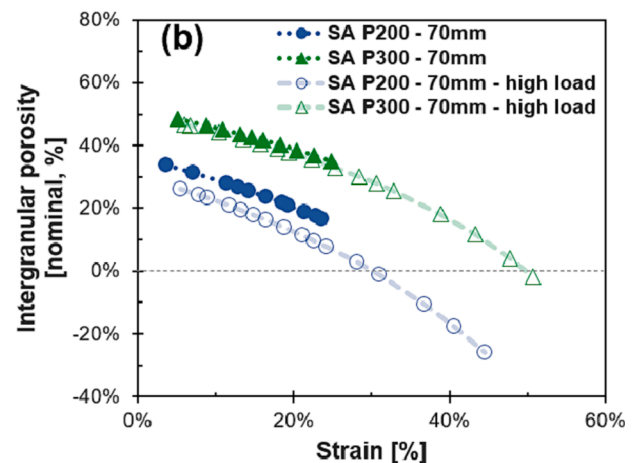
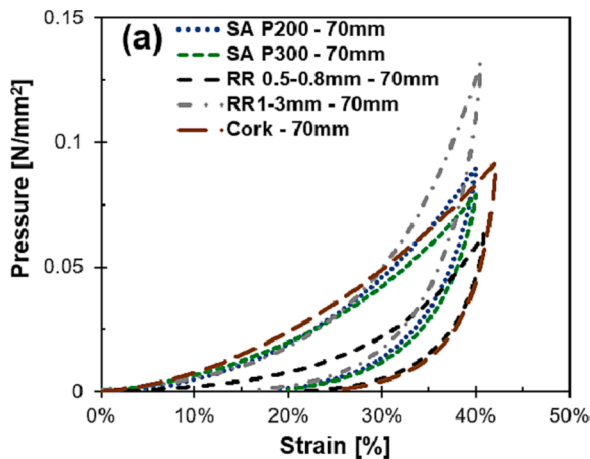


Fig. 12. A) compression-decompression cycles for all materials in 70 mm thickness up to 40% strain. b) Nominal inter-granular porosity during static compression of silica aerogel beds of 70 mm thickness.

The stress relaxation (Fig. 13) and creep strain (Fig. S5) behavior of silica aerogel and rubber granule beds were also evaluated. Stress relaxation was determined after a (rapid) compression from 0 to 40% strain in 3 s followed by a hold time at 40% strain of 60 min (Fig. 13a). The silica aerogel and recycled rubber granule beds both display a rapid initial stress relaxation of about 5–10% during the first 2 s (after established straining of 40%). Because the loading and the initial stress relaxation occur within a short time frame of about 5 s, it is not clear if the data reflect the relaxation of the sample alone, or if the data are affected by a response of the instrument after such a sudden change in conditions. Thus, we do not consider this initial response further. During the subsequent hour at rest with 40% strain, the silica aerogel granule beds show a power-law behavior ($\sigma \sim t^\alpha$, linear on the log-log plot, Fig. 13b) with an equal exponent α of 0.017 (MPa/min). The recycled rubber granule bed does not show such a clear power law behavior, and the overall stress relaxation is higher. Because monolithic silica aerogels of the investigated density behave elastically with fast strain recovery, we hypothesize here that the relaxation behavior of the silica aerogel observed is predominantly a behavior of its form as a packed bed of granules. The mechanism behind this is probably a rearrangement of particles and a reduction in particle size, rather than a feature of the bulk material of the silica aerogel. Separating any relaxation effects of the silica aerogel bulk material itself, which could potentially complement the interpretation of the vibroacoustic data above, is probably not feasible and was not attempted here.

4. Potential of silica aerogels for vibration isolation

Until now, the vibration isolation and damping properties of silica aerogels had not been evaluated systematically. The first dataset from this study, acquired over a wide range in static loads, indicates that silica aerogels outperform recycled rubber granules and expanded cork, and may be competitive with polyurethane foams.

The data indicate that silica aerogels have a low resonance frequency which is below 20 Hz at static loads in a typical range of relevance for application in building floors and under-screed structure-borne sound insulation applications. A further decrease to 15 and even 11 Hz are possible for aerogels with a thickness of 70 mm and at loads beyond 0.010 N/mm². As the load increases up to 0.125 N/mm² and more, the silica aerogels maintain this low resonance frequency. These intermediate and high loads are in the relevant range for application in the foundations of buildings in situations where the building has to be protected against vibrations from the surroundings. Typical solutions for such demanding structure-borne sound vibration isolation applications are currently highly engineered polyurethane foams. While these

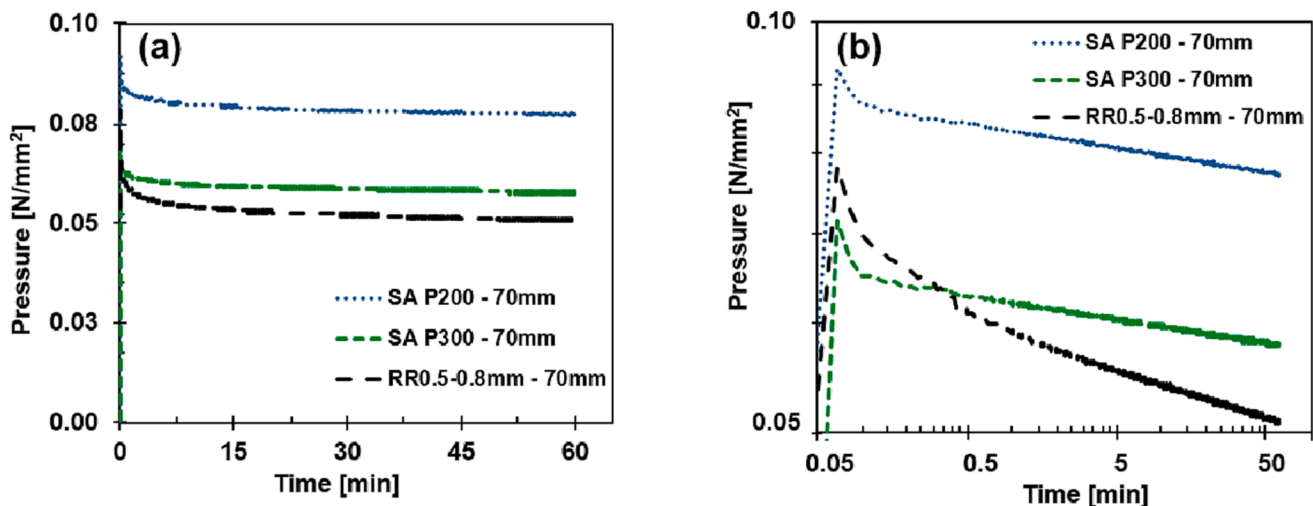


Fig. 13. Stress relaxation after a three-second loading in compression from 0 to 40% strain. (a) the linear plot, (b) log-log plot.

materials do offer high performance, they are expensive and are performing well only in a very narrow band of static loading. This means, that a large portfolio of products, each optimized for a specific static loading, is required to cover the highly variable loads found in building foundations, e.g. very high loads under pillars, high loads under carrying walls, and low to moderate loads elsewhere. Silica aerogels may offer solutions using only a single material covering the vibration insulation over a wide loading range. This would greatly simplify the planning of the vibration isolation concept of buildings. In addition, whilst silica aerogels are not inexpensive itself, there may be a cost-benefit, particularly for the higher loads where the cost of the polyurethane foams rapidly increases. In addition, the ultra-low thermal conductivity of silica aerogels, as low as 0.012 W/(m·K) for a compressed bed of granules [68], may provide an additional benefit: Since in many building projects, additional thermal insulation layers must be installed in addition to the vibration isolation materials. These parts have 4 to 12 times higher thermal conductivities than the silica aerogels, namely on the order of $\sim 0.10 \text{ W/(m·K)}$ for rubber granulate mats, and $0.05\text{--}0.15 \text{ W/(m·K)}$ for vibration-damping polyurethane foams.

Although a simple bed of silica aerogel granules is still far away from a product ready for entering the market, such materials could be used now for special niches of application. Further research and development work is required before market entry can be considered for aerogels including:

- Extended vibroacoustic characterization and simulations beyond the simple 1-DOF framework
- Research targeting mechanistic insights into the cause of the resonance frequency being so low for silica aerogels. The data here indicate that the effect is due to the silica aerogel itself, rather than the bed of granules used here since the performance is insensitive to the porosity between the grains. Vibration damping is often considered in terms of internal friction, which could be high in aerogels due to their large specific surface area. However, our data indicate that the loss factor and the damping ratio are actually low. Currently, we have not yet a clear understanding of the cause of the low resonance frequency of these materials. Potential insights could be gained by more vibroacoustic characterizations of different types of aerogels, having significantly different pore structures and mechanical properties, e.g. silica aerogels with variable density and consequently highly variable compressive stiffness [59,60]. Other materials of interest could be irreversibly compressible nanofibrous cellulose aerogels [69,70], polymethylsilsequioxane, related organo-silica aerogels, and foams with a wide variety of particle and pore sizes and mechanical properties [71–74]. Deeper insight, however, will

probably also require numerical simulations of the dynamic mechanical response of aerogel structures.

Aside from the more scientific questions, there is of course also the challenge of developing products that can satisfy the requirements in terms of static compression, creep, dust release and long-term stability, without deteriorating their vibration isolation performance. Here, we see a wide range of possibilities, including fiber reinforcement [2], aerogel impregnation in foams, the use of binders and/or the combination of silica aerogel granules with other fillers. A good starting point for further promising developments could be a vibroacoustic characterization of current commercial aerogel products optimized for thermal insulation.

5. Conclusions

Silica aerogels, as the most popular industrial aerogels, have attracted the attention of researchers and developers in the industry not only for their record-breaking low thermal conductivity, but increasingly also for their outstanding acoustic properties. Despite the rapidly increasing research on air-borne sound absorption, structure-borne sound, and vibration isolation have not been studied in detail yet. In this study, we have addressed this important knowledge gap and contrasted the performance of silica aerogels to that of recycled rubber and expanded cork. The vibro-acoustic data presented here indicate a very strong potential of aerogel-based materials for vibration isolation: it was revealed that silica aerogels have a low dynamic stiffness and very low resonance frequencies over a wide static load range. The vibration isolation properties outperform those of rubber granules by an order of magnitude, and are similar to those of highly engineered, costly polyurethane foams. Hence, vibration and structure-borne sound isolation has the potential to become a unique selling point of silica aerogel products, perhaps more so than its air-borne sound absorption properties, which are also good, but not exceptional. Further studies on the physical mechanisms behind the observed low resonance frequency, the evaluation of other aerogel materials, and targeted R&D to develop products for the market are still required to make this a reality, including data interpretation beyond the single degree of freedom framework, mechanistic insight through modeling and measurements on other types of aerogels and the use of binders and fibers to produce composites that meet market demands.

CRedit authorship contribution statement

Oriana Palacio: Writing – original draft, Visualization,

Methodology. **Wim J. Malfait:** Writing – review & editing, Supervision, Project administration, Conceptualization. **Silvain Michel:** Writing – review & editing, Validation, Software, Conceptualization. **Michel Barbezat:** Writing – review & editing, Project administration. **Zahra Mazrouei-Sebdani:** Writing – original draft, Writing – review & editing, Visualization, Supervision, Resources, Project administration, Methodology, Investigation, Conceptualization.

Declaration of Competing Interest

The authors declare that they have no known competing financial interests or personal relationships that could have appeared to influence the work reported in this paper.

Data availability

Data will be made available on request.

Acknowledgments

We thank Thomas Bergmann and Daniel Völki for their assistance with the forced vibration measurements, Christopher Knutz for discussions on the data interpretation, Florian Welter for his insights in the vibration isolation market, and Michal Ganobjak for aerogel photography. This project was funded by Empa internal means and supported in part by the Swiss National Science Foundation SNSF (BRIDGE-193700) and Innosuisse (57285.1 IP-EE).

Appendix A. Supplementary data

Supplementary data to this article can be found online at <https://doi.org/10.1016/j.conbuildmat.2023.132568>.

References

- [1] M.A. Aegerter, N. Leventis, M.M. Koebel (Eds.), *Aerogels Handbook*, Springer New York, New York, NY, 2011.
- [2] Z. Mazrouei-Sebdani, M. Naeimirad, S. Petersek, H. Begum, S. Galmarini, F. Pursche, E. Baskin, S. Zhao, T. Gries, W.J. Malfait, Multiple assembly strategies for silica aerogel-fiber combinations—a review, *Mater. Des.* (2022), 111228, <https://doi.org/10.1016/j.matdes.2022.111228>.
- [3] S. Zhao, G. Siqueira, S. Drdova, D. Norris, C. Ubert, A. Bonnin, S. Galmarini, M. Ganobjak, Z. Pan, S. Brunner, Additive manufacturing of silica aerogels, *Nature* 584 (7821) (2020) 387–392, <https://doi.org/10.1038/s41586-020-2594-0>.
- [4] J.P. Vareda, A. Lamy-Mendes, L. Durães, A reconsideration on the definition of the term aerogel based on current drying trends, *Microporous Mesoporous Mater.* 258 (2018) 211–216, <https://doi.org/10.1016/j.micromeso.2017.09.016>.
- [5] S. Groult, S. Buwalda, T. Budtova, Pectin hydrogels, aerogels, cryogels and xerogels: Influence of drying on structural and release properties, *Eur. Polym. J.* 149 (2021), 110386, <https://doi.org/10.1016/j.eurpolymj.2021.110386>.
- [6] J.P. Arenas, M.J. Crocker, Recent trends in porous sound-absorbing materials, *Sound & Vibration* 44 (7) (2010) 12–18.
- [7] S. Ahmad, S. Ahmad, J.N. Sheikh, Silica centered aerogels as advanced functional material and their applications: a review, *J. Non Cryst. Solids* 611 (2023), 122322, <https://doi.org/10.1016/j.jnoncrysol.2023.122322>.
- [8] R. Baetens, B.P. Jelle, A. Gustavsen, Aerogel insulation for building applications: a state-of-the-art review, *Energ. Buildings* 43 (4) (2011) 761–769, <https://doi.org/10.1016/j.enbuild.2010.12.012>.
- [9] A. Lamy-Mendes, A.D.R. Pontinha, P. Alves, P. Santos, L. Durães, Progress in silica aerogel-containing materials for buildings' thermal insulation, *Constr. Build. Mater.* 286 (2021), 122815, <https://doi.org/10.1016/j.conbuildmat.2021.122815>.
- [10] Y. Liu, P. Zheng, H. Wu, Y. Zhang, Preparation and dynamic moisture adsorption of fiber felt/silica aerogel composites with ultra-low moisture adsorption rate, *Constr. Build. Mater.* 363 (2023), 129825, <https://doi.org/10.1016/j.conbuildmat.2022.129825>.
- [11] Y. Chen, S. Sepahvand, F. Gauvin, K. Schollbach, H. Brouwers, Q. Yu, One-pot synthesis of monolithic silica-cellulose aerogel applying a sustainable sodium silicate precursor, *Constr. Build. Mater.* 293 (2021), 123289, <https://doi.org/10.1016/j.conbuildmat.2021.123289>.
- [12] P. Liu, Y.F. Gong, G.H. Tian, Z.K. Miao, Preparation and experimental study on the thermal characteristics of lightweight prefabricated nano-silica aerogel foam concrete wallboards, *Constr. Build. Mater.* 272 (2021), 121895, <https://doi.org/10.1016/j.conbuildmat.2020.121895>.
- [13] J. Gu, R. Fu, S. Kang, X. Yang, Q. Song, C. Miao, M. Ma, Y. Wang, H. Sai, Robust composite aerogel beads with pomegranate-like structure for water-based thermal insulation coating, *Constr. Build. Mater.* 341 (2022), 127722, <https://doi.org/10.1016/j.conbuildmat.2022.127722>.
- [14] N. Bheekhun, A. Talib, A. Rahim, M.R. Hassan, Aerogels in aerospace: an overview, *Adv. Mater. Sci. Eng.* 2013 (2013) 1–18, <https://doi.org/10.1155/2013/406065>.
- [15] Y. Chen-Yang, Y. Wang, Y. Chen, Y. Li, H. Chen, H. Chiu, Influence of silica aerogel on the properties of polyethylene oxide-based nanocomposite polymer electrolytes for lithium battery, *J. Power Sources* 182 (1) (2008) 340–348, <https://doi.org/10.1016/j.jpowsour.2008.04.001>.
- [16] Z. Mazrouei-Sebdani, H. Begum, S. Schoenwald, K.V. Horoshenkov, W.J. Malfait, A review on silica aerogel-based materials for acoustic applications, *J. Non Cryst. Solids* 562 (2021), 120770, <https://doi.org/10.1016/j.jnoncrysol.2021.120770>.
- [17] T. Budtova, T. Lokki, S. Malakooti, A. Rege, H. Lu, B. Milow, J. Vapaavuori, S. L. Vivod, Acoustic properties of aerogels: current status and prospects, *Adv. Eng. Mater.* 25 (2022) 2201137, <https://doi.org/10.1002/adem.202201137>.
- [18] J.Y. Cai, S. Lucas, L.J. Wang, Y. Cao, Insulation properties of the monolithic and flexible aerogels prepared at ambient pressure, *Advanced Materials Research*, Trans Tech Publ (2012) 116–120, <https://doi.org/10.4028/www.scientific.net/AMR.391-392.116>.
- [19] M. Sachithanadam, S.C. Joshi, Effect of granule sizes on acoustic properties of protein-based silica aerogel composites via novel inferential transmission loss method, *Gels* 2 (1) (2016) 11, <https://doi.org/10.3390/gels2010011>.
- [20] H. Begum, K. Horoshenkov, M. Conte, W. Malfait, S. Zhao, M. Koebel, P. Bonfiglio, R. Venegas, The acoustical properties of tetraethyl orthosilicate based granular silica aerogels, *J. Acoust. Soc. Am.* 149 (6) (2021) 4149–4158, <https://doi.org/10.1121/1.50005200>.
- [21] S. Silviana, F. Hermawan, J. Indrachya, D.A.L. Kusumawardhani, F. Dalanta, Optimizing the environmentally friendly silica-cellulose aerogel composite for acoustic insulation material derived from newspaper and geothermal solid waste using a central composite design, *J. Sol-Gel Sci. Technol.* 103 (1) (2022) 226–243, <https://doi.org/10.1007/s10971-022-05831-y>.
- [22] A. Dasyam, Y. Xue, J.S. Bolton, B. Sharma, Effect of particle size on sound absorption behavior of granular aerogel agglomerates, *J. Non Cryst. Solids* 598 (2022), 121942, <https://doi.org/10.1016/j.jnoncrysol.2022.121942>.
- [23] K.W. Oh, D.K. Kim, S.H. Kim, Ultra-porous flexible PET/Aerogel blanket for sound absorption and thermal insulation, *Fibers Polym.* 10 (2009) 731–737, <https://doi.org/10.1007/s12221-010-0731-3>.
- [24] S. Motahari, H. Javadi, A. Motahari, Silica-aerogel cotton composites as sound absorber, *J. Mater. Civ. Eng.* 27 (9) (2015) 04014237, [https://doi.org/10.1061/\(ASCE\)MT.1943-5533.0001208](https://doi.org/10.1061/(ASCE)MT.1943-5533.0001208).
- [25] H. Begum, K.V. Horoshenkov, Acoustical properties of fiberglass blankets impregnated with silica aerogel, *Appl. Sci.* 11 (10) (2021) 4593, <https://doi.org/10.3390/app11104593>.
- [26] Z. Talebi, P. Soltani, N. Habibi, F. Latifi, Silica aerogel/polyester blankets for efficient sound absorption in buildings, *Constr. Build. Mater.* 220 (2019) 76–89, <https://doi.org/10.1016/j.conbuildmat.2019.06.031>.
- [27] Z. Mazrouei-Sebdani, A. Khodami, H. Hadadzadeh, M. Zarrebini, Synthesis and performance evaluation of the aerogel-filled PET nanofiber assemblies prepared by electro-spinning, *RSC advances* 5(17) (2015) 12830–12842. DOI 0.1039/C4RA15297B.
- [28] V. Gibiat, O. Lefeuvre, T. Woignier, J. Pelous, J. Phalippou, Acoustic properties and potential applications of silica aerogels, *J. Non Cryst. Solids* 186 (1995) 244–255, [https://doi.org/10.1016/0022-3093\(95\)00049-6](https://doi.org/10.1016/0022-3093(95)00049-6).
- [29] C. Buratti, E. Belloni, E. Lascaro, F. Merli, P. Ricciardi, Rice husk panels for building applications: thermal, acoustic and environmental characterization and comparison with other innovative recycled waste materials, *Constr. Build. Mater.* 171 (2018) 338–349, <https://doi.org/10.1016/j.conbuildmat.2018.03.089>.
- [30] A. Kueh, A. Razali, Y. Lee, S. Hamdan, I. Yakub, N. Suhaili, Acoustical and mechanical characteristics of mortars with pineapple leaf fiber and silica aerogel in-fills—Measurement and modeling, *Mater. Today Commun.* 35 (2023), 105540, <https://doi.org/10.1016/j.mtcomm.2023.105540>.
- [31] A. Geslain, J.-P. Groby, V. Romero-García, F. Cervera, J. Sánchez-Dehesa, Acoustic characterization of silica aerogel clamped plates for perfect absorption, *J. Non Cryst. Solids* 499 (2018) 283–288, <https://doi.org/10.1016/j.jnoncrysol.2018.07.021>.
- [32] M. Djenane, R. Demagh, F. Hammoud, Rotation of stresses in french wheel tracking test, *Civil Eng. J.* 8 (3) (2022) 438–453, <https://doi.org/10.28991/CEJ-2022-08-03-03>.
- [33] O. Hänninen, A.B. Knol, M. Jantunen, T.-A. Lim, A. Conrad, R. Rappolder, P. Carrer, A.-C. Fanetti, R. Kim, J. Buekers, Environmental burden of disease in Europe: assessing nine risk factors in six countries, *Environ. Health Perspect.* 122 (5) (2014) 439–446, <https://doi.org/10.1289/ehp.1206154>.
- [34] W.H. Organization, *Environmental noise guidelines for the European region*, World Health Organization, Regional Office for Europe, 2018.
- [35] M. Brink, B. Schäffer, D. Vienneau, R. Pieren, M. Foraster, I.C. Eze, F. Rudzik, L. Thiesse, C. Cajochen, N. Probst-Hensch, Self-reported sleep disturbance from road, rail and aircraft noise: exposure-response relationships and effect modifiers in the SIRENE study, *Int. J. Environ. Res. Public Health* 16 (21) (2019) 4186, <https://doi.org/10.3390/ijerph16214186>.
- [36] E. Peris, J. Woodcock, G. Sica, A. Moorhouse, D. Waddington, Annoyance from railway vibration in residential environments: factors of importance when considering exposure-response relationships, *J. Acoust. Soc. Am.* 131 (4) (2012) 3504, <https://doi.org/10.1121/1.4709242>.
- [37] S.H. Park, P.J. Lee, Effects of floor impact noise on people—annoyance and physiological responses, 12th ICBCN Congress on Noise as a Public Health Problem, Zurich, 2017.

- [38] T. Bangia, R. Raskar, Cohesive methodology in construction of enclosure for 3.6 m devasthal optical telescope, *HighTech Innov. J.* 3 (2) (2022) 162–174, <https://doi.org/10.28991/HIJ-2022-03-02-05>.
- [39] B.C. Chakraborty, D. Ratna, *Polymers for vibration damping applications*, Elsevier, 2020.
- [40] G. Müller, M. Möser (Eds.), *Handbook of Engineering Acoustics*, Springer Berlin Heidelberg, Berlin, Heidelberg, 2013.
- [41] M. Etchessahar, S. Sahraoui, L. Benyahia, J. Tassin, Frequency dependence of elastic properties of acoustic foams, *J. Acoust. Soc. Am.* 117 (3) (2005) 1114–1121, <https://doi.org/10.1121/1.1857527>.
- [42] B. Yang, *Vibration analysis of one-degree-of-freedom systems*, in: B. Yang (Ed.), *Stress, Strain, and Structural Dynamics*, (Second Edition), Academic Press, 2023, pp. 431–528.
- [43] S.H. Crandall, The role of damping in vibration theory, *J. Sound Vib.* 11 (1) (1970) 3–18, [https://doi.org/10.1016/S0022-460X\(70\)80105-5](https://doi.org/10.1016/S0022-460X(70)80105-5).
- [44] E.E. Ungar, Damping of structures and use of damping materials, *Handbook of Noise and Vibration Control* (2007) 734–744, <https://doi.org/10.1002/9780470209707.ch60>.
- [45] R. Ibrahim, Recent advances in nonlinear passive vibration isolators, *J. Sound Vib.* 314 (3–5) (2008) 371–452, <https://doi.org/10.1016/j.jsv.2008.01.014>.
- [46] C.F. Beards, The vibrations of systems having one degree of freedom, in: C. F. Beards (Ed.), *Engineering Vibration Analysis With Application to Control Systems*, Butterworth-Heinemann, 1995, pp. 10–87.
- [47] B. Yang, *Theory of Vibration | Fundamentals*, in: S. Braun (Ed.), *Encyclopedia of Vibration*, Elsevier, 2001, pp. 1290–1299.
- [48] R.G. Wettschreck, Vibration and structure-borne sound isolation by means of cellular polyurethane (PUR) elastomers, *Vibrationsdagen (SVIB)*, Stockholm, Proc. SVIB-Vibrationsdagen, 1994, pp. 21–52.
- [49] S.Y. Yoo, J.Y. Jeon, Investigation of the effects of different types of interlayers on floor impact sound insulation in box-frame reinforced concrete structures, *Build. Environ.* 76 (2014) 105–112, <https://doi.org/10.1016/j.buildenv.2014.03.008>.
- [50] C.W. Shan, M.I. Ghazali, M.I. Idris, Improved vibration characteristics of flexible polyurethane foam via composite formationenglish, *Int J Automot Mech Eng* 7 (2013) 1031–1042.
- [51] M. Gatto, L. Montrasio, A. Tsinaris, D. Pitilakis, A. Anastasiadis, *The dynamic behaviour of polyurethane foams in geotechnical conditions*, CRC Press, *Earthquake Geotechnical Engineering for Protection and Development of Environment and Constructions*, 2019, pp. 2566–2573.
- [52] T. Bose, D. Choudhury, J. Sprengel, M. Ziegler, Efficiency of open and infill trenches in mitigating ground-borne vibrations, *J. Geotech. Geoenviron. Eng.* 144 (8) (2018) 04018048, [https://doi.org/10.1061/\(ASCE\)GT.1943-5606.0001915](https://doi.org/10.1061/(ASCE)GT.1943-5606.0001915).
- [53] M. Sambucci, M. Valente, Influence of waste tire rubber particles size on the microstructural, mechanical, and acoustic insulation properties of 3D-printable cement mortars, *Civ. Eng. J* 7(6) (2021) 937. 10.28991/cej-2021-03091701.
- [54] B. Marques, J. Antonio, J. Almeida, A. Tadeu, J. de Brito, S. Dias, F. Pedro, J. D. Sena, Vibro-acoustic behaviour of polymer-based composite materials produced with rice husk and recycled rubber granules, *Constr. Build. Mater.* 264 (2020), 120221, <https://doi.org/10.1016/j.conbuildmat.2020.120221>.
- [55] A. Calabrese, D. Losanno, M. Spizzuoco, S. Strano, M. Terzo, Recycled rubber fiber reinforced bearings (RR-FRBs) as base isolators for residential buildings in developing countries: the demonstration building of Pasir Badak, Indonesia, *Eng. Struct.* 192 (2019) 126–144, <https://doi.org/10.1016/j.engstruct.2019.04.076>.
- [56] A. Calabrese, M. Spizzuoco, G. Serino, G. Della Corte, G. Maddaloni, Shaking table investigation of a novel, low-cost, base isolation technology using recycled rubber, *Struct. Control Health Monit.* 22 (1) (2015) 107–122, <https://doi.org/10.1002/stc.1663>.
- [57] R. Nayak, R. Padhye, *Acoustic textiles: an introduction*, *Acoustic Textiles* (2016) 1–32.
- [58] Z. Mazrouei-Sebdani, A. Khoddami, H. Hadadzadeh, M. Zarrebini, A. Karimi, F. Shams-Ghahfarokhi, The effect of the nano-structured aerogel powder on the structural parameters, water repellency, and water vapor/air permeability of a fibrous polyester material, *Mater. Chem. Phys.* 177 (2016) 99–111, <https://doi.org/10.1016/j.matchemphys.2016.04.002>.
- [59] J.C. Wong, H. Kaymak, S. Brunner, M.M. Koebel, Mechanical properties of monolithic silica aerogels made from polyethoxydisiloxanes, *Microporous Mesoporous Mater.* 183 (2014) 23–29, <https://doi.org/10.1016/j.micromeso.2013.08.029>.
- [60] D. Sivaraman, S. Zhao, S. Iswar, M. Lattuada, W.J. Malfait, Aerogel spring-back correlates with strain recovery: effect of silica concentration and aging, *Adv. Eng. Mater.* 23 (10) (2021) 2100376, <https://doi.org/10.1002/adem.202100376>.
- [61] G. Reichenauer, Structural characterization of aerogels, in: M.A. Aegerter, N. Lentitis, M.M. Koebel (Eds.), *Aerogels Handbook*, Springer, New York, 2011, pp. 449–498, https://doi.org/10.1007/978-1-4419-7589-8_21.
- [62] K. Nering, A. Kowalska-Koczwara, Determination of vibroacoustic parameters of polyurethane mats for residential building purposes, *Polymers* 14 (2) (2022) 314, <https://doi.org/10.3390/polym14020314>.
- [63] S.I. Hayek, *Mechanical vibration and damping*, *Digital Encyclopedia of Applied Physics* (2003).
- [64] S.S. Rao, *Vibration of Continuous Systems*, John Wiley & Sons, 2019.
- [65] C.W. To, *Introduction to Dynamics and Control in Mechanical Engineering Systems*, John Wiley & Sons, 2016.
- [66] L. Meirovitch, *Fundamentals of Vibrations*, Waveland Press, US, 2010.
- [67] Z. Qu, M. Sheng, Determination of Dynamic Mechanical Properties of Silica Aerogel by Resonance and Non-Resonance Method, in: *IOP Conference Series: Materials Science and Engineering*, IOP Publishing, 2017, p. 012035, <https://doi.org/10.1088/1757-899X/182/1/012035>.
- [68] A. Neugebauer, K. Chen, A. Tang, A. Allgeier, L.R. Glicksman, L.J. Gibson, Thermal conductivity and characterization of compacted, granular silica aerogel, *Energ. Buildings* 79 (2014) 47–57, <https://doi.org/10.1016/j.enbuild.2014.04.025>.
- [69] S.F. Plappert, J.-M. Nedelec, H. Rennerhofer, H.C. Lichtenegger, F.W. Liebner, Strain hardening and pore size harmonization by uniaxial densification: a facile approach toward superinsulating aerogels from nematic nanofibrillated 2, 3-dicarboxyl cellulose, *Chem. Mater.* 29 (16) (2017) 6630–6641, <https://doi.org/10.1021/acs.chemmater.7b00787>.
- [70] D. Sivaraman, G. Siqueira, A.K. Maurya, S. Zhao, M.M. Koebel, G. Nyström, M. Lattuada, W.J. Malfait, Superinsulating nanocellulose aerogels: effect of density and nanofiber alignment, *Carbohydr. Polym.* 292 (2022), 119675, <https://doi.org/10.1016/j.carbpol.2022.119675>.
- [71] A.V. Rao, S.D. Bhagat, H. Hirashima, G. Pajonk, Synthesis of flexible silica aerogels using methyltrimethoxysilane (MTMS) precursor, *J. Colloid Interface Sci.* 300 (1) (2006) 279–285, <https://doi.org/10.1016/j.jcis.2006.03.044>.
- [72] Y. Aoki, T. Shimizu, K. Kanamori, A. Maeno, H. Kaji, K. Nakanishi, Low-density, transparent aerogels and xerogels based on hexylene-bridged polysilsesquioxane with bendability, *J. Sol-Gel Sci. Technol.* 81 (2017) 42–51, <https://doi.org/10.1007/s10971-016-4077-1>.
- [73] G. Zu, K. Kanamori, X. Wang, K. Nakanishi, J. Shen, Superelastic triple-network polyorganosiloxane-based aerogels as transparent thermal superinsulators and efficient separators, *Chem. Mater.* 32 (4) (2020) 1595–1604, <https://doi.org/10.1021/acs.chemmater.9b04877>.
- [74] L. Huber, S.B. Hauser, C.J. Ubert, M. Rees, B. Fischer, S. Zhao, M.M. Koebel, W. J. Malfait, Surfactant-free, flexible polymethylsilsesquioxane foams, *J. Non Cryst. Solids* 597 (2022), 121887, <https://doi.org/10.1016/j.jnoncrysol.2022.121887>.